

Multivalent cations modulating microstructure and interactions of potato protein and fungal hyphae in a functional meat analogue

Mary C. Okeudo-Cogan^{a,b}, Shuyue Yang^b, Brent S. Murray^{b,*}, Rammile Ettelaie^b, Simon D. Connell^c, Stewart Radford^e, Stuart Micklethwaite^a, Yoselin Benitez-Alfonso^d, Richa Yeshvekar^d, Anwesha Sarkar^{b,*}

^a School of Chemical and Process Engineering, University of Leeds, Leeds, LS2 9JT, UK

^b Food Colloids and Bioprocessing Group, School of Food Science and Nutrition, University of Leeds, Leeds, LS2 9JT, UK

^c School of Physics and Astronomy, University of Leeds, Leeds, LS2 9JT, UK

^d Centre for Plant Sciences, The Astbury Centre, School of Biology, University of Leeds, Leeds, LS2 9JT, UK

^e Quorn Foods, Station Road, Stokesley, North Yorkshire, TS9 7AB, UK

ARTICLE INFO

Keywords:

Meat analogues
Ferric pyrophosphate fortification
Plant protein
Fungi biomass
Storage modulus

ABSTRACT

Concentrated *Fusarium venenatum* biomass commonly known as mycoprotein (*MYC*), naturally rich in high quality proteins, has been commercially used to fabricate vegan meat analogues by incorporating potato protein (*PoP*). In this work, we studied the effect of multivalent cations, focusing particularly on essential micronutrients such as calcium (0–100 mM) and ferric ions (0–1.0 mM), on the microstructure of the fungal hyphae (*MYC*)-*PoP* composites, as characterized via rheology and microscopic techniques as a function of pH (3.0–7.0), Na⁺ (0–200 mM) with and without added *PoP*. A clear dependency of storage modulus (*G'*) on pH, ionic strength and specific concentrations of Ca²⁺ and Fe³⁺ was observed, with Fe³⁺, *PoP* concentration and acidic pH having the largest impact. Microscopy across various length scales revealed that *PoP* coats the hyphae's rough surface and dominates the interactions between the hyphae. *G'* responsiveness to NaCl and CaCl₂ concentrations indicated that electrostatic interactions between the fungal hyphae and *PoP* coverage mainly govern texture properties. Interestingly, Fe³⁺ induced protein-protein aggregation which led to a reduction in *G'* of *MYC* without *PoP*. However, the effect of Fe³⁺ was modulated by Ca²⁺, where increasing concentration of both salts seemed to narrow the rheological (*G'*) differences between *MYC* with and without *PoP* at higher pH. Fe³⁺ alone significantly increased the *G'* of *MYC*-*PoP* except at pH 5.0. Thus, a subtle balancing of pH and added levels of calcium is needed to enable iron supplementation with minimal textural effects when formulating mycoprotein-based meat analogues with *PoP* as protein binding agent.

1. Introduction

Animal-derived meat has been an integral part of human diet over our evolutionary history and is a rich source of proteins, fats, vitamins and minerals (Baltic & Boskovic, 2015). Nutrient analysis of raw good quality beef cuts by Desimone et al. (2013) showed that 100 g of raw beef has 18–23 g protein, 5.2–12 g fat, 74 mg cholesterol and 3.8 µg vitamin B12. This makes animal meat an important source of micronutrients such as bioavailable haem iron and vitamin B12 that are absent, or are present with limited bioavailability, in most meat analogues/alternatives (MAs) (Cabrera, Ramos, Saadoun, & Brito, 2010;

Desimone et al., 2013; Finnigan et al., 2019). Research and development of MAs has mostly focused on good quality protein sources that mimic traditional animal muscle meat attributes whilst having little to moderate processing and being 'sustainably' derived to meet consumer preferences. The moderate to high protein content and relatively lower fat level provide some nutritional improvement of MAs over traditional meat. However, their lower micronutrient quality raises the challenge of nutrient intake in individuals who aim to completely replace traditional meats with MAs fabricated with alternative proteins. This nutrition concern is therefore driving food industries and researchers to understand the effects of fortification of iron, zinc and vitamin B12 in

* Corresponding author.

** Corresponding author.

E-mail addresses: B.S.Murray@leeds.ac.uk (B.S. Murray), A.Sarkar@leeds.ac.uk (A. Sarkar).

<https://doi.org/10.1016/j.foodhyd.2023.109569>

Received 23 August 2023; Received in revised form 31 October 2023; Accepted 15 November 2023

Available online 18 November 2023

0268-005X/© 2023 The Authors. Published by Elsevier Ltd. This is an open access article under the CC BY license (<http://creativecommons.org/licenses/by/4.0/>).

commercially available MAs (Melville, et al., 2023).

The filamentous fungus *Fusarium venenatum*, at a biomass of roughly 20% solids content, commonly known as mycoprotein (MYC), has been commercially used to fabricate MAs for more than four decades (Finnigan, Needham, & Abbott, 2017; Wiebe, 2004). MYC is rich in high quality proteins and some micronutrients with a nutrient profile of 11.5 g of protein, 2.9 g of total fat, 1.7–3.0 g of total carbohydrate, 6 g of dietary fibre, 0 µg vitamin B12, 9 mg of zinc and 0.5 mg of iron per 100 g wet weight (Finnigan, 2011; Finnigan et al., 2019). Often proteins such as egg white protein (EWP), at a concentration of about 3 wt %, are used as a functional ingredient, i.e., as a binder of fungal hyphae in MYC-EWP MAs (Finnigan, 2011; Okeudo-Cogan, et al., 2023). Okeudo-Cogan, et al. (2023) demonstrated that EWP coats the MYC surface and gives desirable rheological properties by modulating the effects of monovalent as well as divalent ions and pH conditions in fungal-based MAs. The growing demand for plant-based alternatives to animal proteins as well as egg allergenicity are some of the factors driving the replacement of EWP with plant proteins. Potato protein (PoP) has been chosen to replace EWP in the commercial fungi-based MAs due to its high solubility compared to many other plant proteins (Kew, Holmes, Stieger, & Sarkar, 2021) and the similarities in the viscoelastic properties of patatin gels compared to those of ovalbumin (Creusot, Wierenga, Laus, Giuseppin, & Gruppen, 2011; Hussain et al., 2021). Patatin is the principal protein fraction in most commercial potato varieties but, depending on the potato cultivar, the protein content varies widely: between 40 and 60% patatin, 20–30% protease inhibitors and other high molecular weight proteins making up to 10% of total protein in PoP (Grubben, van Heeringen, & Keesman, 2019). Patatin is a glycoprotein with 366–386 amino acids, a molecular weight of 40–45 kDa and isoelectric point of 4.5–5.1, comparable to ovalbumin which has a molecular weight of 45 kDa, 385 amino acids and an isoelectric point of 4.5 (Andlinger, Röscheisen, Hengst, & Kulozik, 2021; Bevan et al., 1986; Guha, Majumder, & Mine, 2019). Both of these proteins have a similar number of charged groups: 32 and 35 amine groups: 43 and 47 carboxylic groups, in patatin and ovalbumin, respectively. There are significant differences in their sulfhydryl (SH) group and disulphide bridge (S–S) contents, with ovalbumin having four –SH groups and one S–S bridge while patatin has one –SH group and no internal S–S bridges (Andlinger, et al., 2021; Creusot et al., 2011). In this study we characterised for the first time the effect of potato protein at 3 wt % and added salts on the interactions and microstructure of MYC.

Although being generally nutrient-rich, MYC's iron level at 0.5 mg per 100 g wet weight is only 11–36% of the iron content of raw beef: at 1.4–4.6 mg iron per 100 g (Cabrera, et al., 2010; Czerwonka & Tokarz, 2017). The recommended average dietary intake (RDI) of iron for adult females and males aged between 19 and 50 years is 8 and 18 mg, respectively (Institute of Medicine Committee, 1993). This necessitates adequate iron fortification in MYC and therefore an understanding of any effects of such fortification on the microstructural and textural properties of MAs. Ferric pyrophosphate – $\text{Fe}_4(\text{P}_2\text{O}_7)_3$ (FePP) is one of the commonly used iron fortificants in foods, alongside ferrous sulphate, ferrous fumarate and electrolytic iron powder, etc. (Moretti, et al., 2006). FePP has been shown to have a lower impact on the sensory properties of foods due to its reduced solubility in water (Cercamondi, et al., 2016; Moretti et al., 2006). However, it is well known that trivalent cations (i.e., like Fe^{3+}) may affect the behaviour and viscoelastic properties of biopolymers. For instance, bidentate complexation of Fe^{3+} ions by carboxylate groups has been shown to induce stronger gels resulting from heterogeneous aggregation of charged polysaccharides (Sharratt, et al., 2021). Fe^{3+} has been shown to increase the gel strength and reduce the cohesiveness of potato starch gels (Chen, et al., 2014), whilst it also reduces hardness and the water holding capacity of egg white gels (Hou, et al., 2021).

Therefore, this study aimed to investigate the effect of ferric salt fortification on the physical, microstructural and rheological properties of MYC and plant protein composites fabricated using PoP. Sodium

chloride (NaCl) is routinely added to foods as a flavour and taste enhancer (Okeudo-Cogan, et al., 2023) and divalent salts such as calcium chloride (CaCl_2) are frequently added to protein gels to improve their techno-functional properties such as texture, gel strength, water holding capacity emulsification, viscosity foaming capacity stability, among others. Consequently, both NaCl and CaCl_2 were studied alongside Fe^{3+} , but also because both NaCl and CaCl_2 have been shown to impact the rheological and textural properties of protein-polysaccharide composite gels in other recent work on MYC-based gels (Okeudo-Cogan, et al., 2023) at various pH values.

It should be emphasized that the MYC-PoP composites studied, plus the various cations added, merely represent a simplified model system of any actual MAs based on these ingredients. (Comparison with actual commercial MA products or real meat are therefore out of scope). It excludes other possible flavour and nutrient additions as well as the effects of further processing – although we hope to include some processing effects in future work. Nevertheless, the combinations chosen should provide a firm foundation for understanding the behaviour of the key ingredients (MYC and PoP) when the most important salts are added.

2. Materials and methods

2.1. Materials

Chilled fungal hyphae paste (MYC) at approximately 24% solids and Solanic® 200 potato protein (PoP) were supplied by Quorn Foods (Stokesley, North Yorkshire, UK). MYC was flash frozen in liquid nitrogen and stored at -80°C . When required, the frozen MYC was thawed at room temperature in a closed container to prevent water loss. Calcofluor White Stain was purchased from Sigma-Aldrich (Dorset, UK). Soluble ferric pyrophosphate was purchased from Merck Life Sciences (Dorset, UK). Polyclonal anti-patatin antibody raised in rabbit was purchased from Agrisera (Vännäs, Sweden). A suitable rabbit secondary antibody conjugated to Alexa 568 dye for anti-patatin was purchased from Thermo Fisher Scientific (Loughborough, UK). Distilled water and analytical grade chemicals were used in the preparation of all samples unless otherwise specified.

2.2. Preparation of MYC and MYC-PoP models

All MYC samples were prepared at 20 wt % solids, by addition of the appropriate amount of distilled water and stirred to achieve a uniform paste. MYC-PoP samples contained 3 wt % added PoP, unless otherwise stated. This was chosen to mimic fungal hyphae and added protein levels in the commercial product (Okeudo-Cogan, et al., 2023). MYC and MYC-PoP composites were prepared at the same combinations of NaCl, CaCl_2 and FePP and at three pH values (pH 3.0, 5.0, 7.0). NaCl concentrations were 0, 100, 200 mM; CaCl_2 concentrations were 0, 50 and 100 mM; $\text{Fe}_4(\text{P}_2\text{O}_7)_3$ concentrations were 0, 0.5 and 1.0 mM. This gave a total of 162 samples for MYC and MYC-PoP. These salt (NaCl and CaCl_2) and pH combinations were selected to cover the typical conditions in the commercial product but also included some more extreme combinations to test for mechanistic understanding. The concentration of FePP at 0.5 mM was chosen such that 100 g of sample contains up to 8 mg of iron, the RDI for an adult male aged between 19 and 50 years (Institute of Medicine Committee, 1993). In fact only about 25% of the total mass of FePP reflects the true mass of iron (Micheletto, et al., 2022). For clarity, FePP at 0.5 mM is 37.3 mg of salt per 100 g of sample, which means that only about 9.3 mg of iron is present in 100 g of sample if 100% solubility is achieved. The reduced solubility and bioavailability of iron from FePP implies that available iron is much lower than 9.3 mg/100 g of sample. As with the monovalent and divalent salts, the more extreme level of FePP of 1.0 mM was selected to substantiate further any changes induced by ferric iron.

2.3. Cryo-scanning electron microscopy (Cryo-SEM) and energy dispersive spectroscopy analysis (EDX)

The microstructures of *MYC* and *MYC-PoP* samples at pH 3.0 and 5.0 were analysed with an FEI Helios G4 CX Dual Beam™ cryo-scanning electron microscope (FEI, Oregon, USA). The elemental microanalysis of image sections was obtained using energy dispersive X-ray spectroscopy (EDX) with an Aztec Energy EDS system (Oxford Instruments, Oxfordshire, UK) with a 150 mm X-max Silicon drift detector (SDD). The sample preparation and imaging methods used were as detailed by Okeudo-Cogan, et al. (2023). Small amounts of sample were mixed with carbon at the optimum cutting temperature for the compound and pressed into a sample holder. The sample holder was then flash frozen in slushed liquid nitrogen at $-207\text{ }^{\circ}\text{C}$. The frozen sample was fractured to expose inner structures, sublimed *via* a thermal cycle to expose more of the hyphae and then coated in iridium to mitigate charging effects by creating a conductive layer. Sample images were taken at 2 kV and 0.1 nA at different magnifications.

2.4. Rheological measurements

Frequency (f) sweeps between 0.01 and 10 Hz, at a constant strain amplitude of 0.1%, were carried out using 25 mm diameter stainless steel serrated parallel plates on an Anton Paar MCR 302 Rheometer (Anton Paar, Ostfildern, Germany) for all *MYC* and *MYC-PoP* composites. About 1.0 g of sample was loaded onto the geometry with gap-size set to 0.650 mm for all experiments. The equipment temperature set to $25\text{ }^{\circ}\text{C}$, and the sample hood lowered during all experiments to limit environmental interference. The storage modulus, G' , was chosen to compare all samples due to the dominance of the elastic properties of the paste, i.e., in all cases $G' > G''$ (loss modulus) (Okeudo-Cogan, et al., 2023).

2.5. Confocal laser scanning microscopy (CLSM)

A Zeiss LSM880 high resolution inverted confocal laser scanning microscope (Zeiss Inc., Heidenheim, Germany) was used to image immuno-labelled *MYC-PoP* dispersions. *MYC-PoP* dispersions were prepared by stirring *MYC* into a solution of *PoP* in phosphate buffered saline (PBS) at pH 7.4, giving a final concentration of 0.1 g L^{-1} and 1.0 g L^{-1} of *MYC* and *PoP* respectively. After incubating for 2 h at room temperature, 1 mL of the dispersion was passed through $0.22\text{ }\mu\text{m}$ nylon filter to collect the *PoP* coated hyphae. The filter holding the hyphae was then incubated in a blocking solution of 5% bovine serum albumin (BSA) in PBS for 2 h - to block non-protein binding sites on the hyphae limiting non-specific binding of the antibodies. This was then washed four times with 10 mL PBS buffer. 1 mL of anti-patatin antibody diluted 1:100 in 5% BSA was added and incubated overnight at $4\text{ }^{\circ}\text{C}$. The hyphae collected on the filter were washed three times using 10 mL PBS buffer. The following steps were carried out in the dark to prevent dye bleaching. The hyphae were incubated with the rabbit secondary antibody conjugated to Alexa 568 dye diluted to 1:100 with 5% BSA for 2 h and then washed four times with 10 mL PBS. The hyphae were counterstained with 0.1 % Calcofluor White (stains all β -glucans in fungal hyphae) diluted 1:10 in PBS for 10 min and then washed four times with 10 mL PBS. Labelled hyphae were back washed using PBS from the filter and imaged in solution using welled coverslip slides. CLSM images were acquired by selective excitation at wavelengths of 405 nm and 578 nm for Calcofluor White and Alexa 568 dyes, respectively.

2.6. Particle size measurements

The mean hydrodynamic diameter (d_H) of *PoP* (0.2 mg/mL in water) with and without added 1.0 mM $\text{Fe}_4(\text{P}_2\text{O}_7)_3$ at pH 3.0, 5.0 and 7.0 were measured using a Malvern Zetasizer Ultra (Malvern instruments Ltd, Worcestershire, UK). 2 mL of each sample was placed in DTS0012

disposable cuvettes (PMMA, Wertheim, Germany). All samples were filtered through a $0.22\text{ }\mu\text{m}$ nylon syringe filter. Samples were equilibrated at $25\text{ }^{\circ}\text{C}$ for 120 s and analysed at a detection angle of 173° using backscattered light. The refractive index of the protein was set at 1.45.

2.7. Statistical analysis

Means and standard deviations were calculated from measurements in triplicate. One-way ANOVA and either Welsh's test; Games-Howell comparison test for the rheology data and post-hoc Tukey for particle size data at 5% level of significance were used to calculate mean separation using Minitab® 21 software.

3. Results & discussion

Firstly, we investigated the effects of the addition of *FePP* to *MYC* at different pH and added CaCl_2 and NaCl , i.e., in the absence of *PoP*, to aid understanding of the effects when *PoP* was included as well, as described in the later sections.

3.1. Characteristics of *MYC* as a function of pH and multivalent salts

Fig. 1 shows the visible changes in colour and structure (classified as pasty or granular) of *MYC* as a function of pH, salt and ionic concentrations. At pH 7.0 and 5.0, *MYC* had a pasty or continuous dough-like appearance at all added salt concentrations. At pH 3.0, *MYC* had a more granular appearance with a loss of clear fluid (i.e., syneresis), when subjected to pressure or shear under most conditions studied, with an exception being *MYC* with 100 mM $\text{CaCl}_2 + 200\text{ mM NaCl}$. A diminishing of the granular structure was observed at this pH whilst an increase in visual granularity was observed with increasing levels of *FePP*. The addition of *FePP* to *MYC* obviously increases the reddish-brown colour, whilst at pH 3.0 CaCl_2 appeared to have a whitening effect on the colour of *MYC + FePP*. This effect seemed to be dependent on the overall ionic composition, with increasing reduction of the reddish-brown colour observed in *MYC* with 1.0 mM *FePP* + 50 mM and 100 mM CaCl_2 , respectively. In general, a lighter/whiter colour is seen with acidification of most samples, with the deepest and lightest colours being observed at pH 7.0 and 3.0, respectively, irrespective of CaCl_2 and *FePP* content. An opposite trend is observed for *MYC* with 1.0 mM *FePP* and 100 mM CaCl_2 , where the deepest hue is observed at pH 3.0, with lighter colours occurring with increasing pH.

The colour change observed with the addition of *FePP* can be attributed to the formation of soluble complexes of ferric and pyrophosphate ions, shown to vary in a pH dependent manner, with minimum soluble complexes formed between pH 4.0 and 6.0 (Tian, Blanco, Smoukov, Veleev, & Velikov, 2016). This also explains the deeper hues observed at pH 7.0 for both concentrations of *FePP*. Thus the decrease in reddish-brown colour with acidification and increase in CaCl_2 concentration suggests that both conditions reduce the solubility of *FePP* and/or sequestration of ferric ions in complex interactions between calcium salts, carboxylate groups and the fungal biomass (Sharratt, et al., 2021). In addition to this, the observed whitening/lightening at pH 3.0 may also be enhanced by the visual structural agglomeration of the fungal hyphae mediated by the 'native' fungal proteins on the hyphal surface, enhanced by *FePP* but reduced by CaCl_2 .

The effect of pH and salts on *MYC* microstructure was studied using cryo-SEM. In Fig. 2, the cryo-SEM micrographs show that the fungal hyphae possess slight surface 'webbing'. These features are probably artefacts of the sample preparation method but certainly there were no obvious changes in the hyphal surface, alignment or inter-hyphal properties of *MYC*, irrespective of levels of added salts and pH, apart from a couple of exceptions. These exceptions were *MYC* at pH 3.0 with 100 mM CaCl_2 and 200 mM NaCl where there was what appeared to be solid sheets between the hyphae and a reduction in the 'webbing' artefacts. However, these are believed to consist of frozen fungal proteins

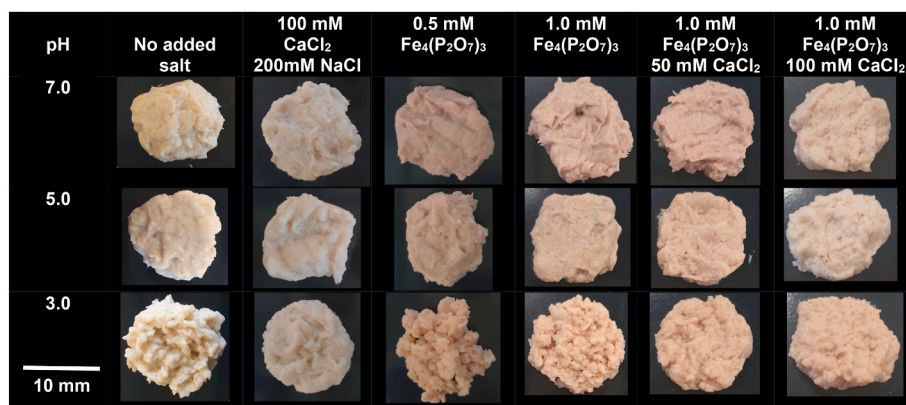


Fig. 1. Macroscopic images of 20 wt % MYC showing changes in colour and visual structure as a function of pH, ionic concentration and salt. Scale bar represents 10 mm.

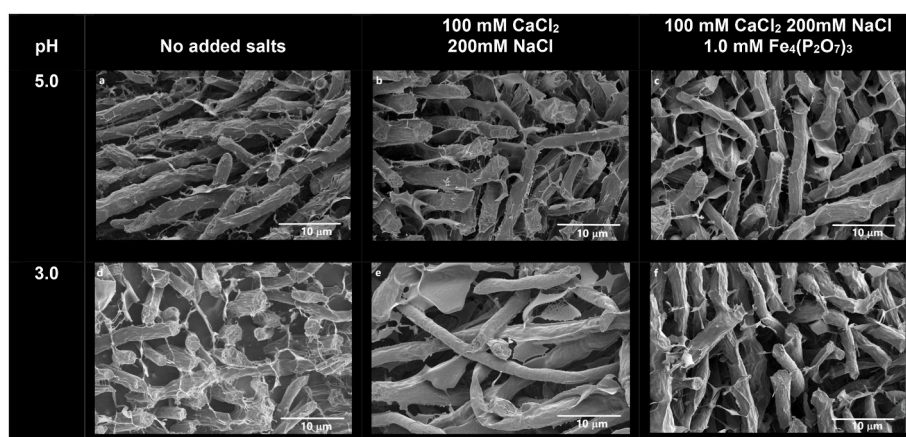


Fig. 2. Cryo-SEM image of MYC (20 wt %) at pH 5.0 with a) no added salts, b) added 200 mM NaCl and 100 mM CaCl₂, c) added 200 mM NaCl, 100 mM CaCl₂ and 1.0 mM Fe₄(P₂O₇)₃; at pH 3.0 with d) no added salts, e) added 200 mM NaCl and 100 mM CaCl₂, f) added 200 mM NaCl, 100 mM CaCl₂ and 1.0 mM Fe₄(P₂O₇)₃. Scale bar represents 10 μm.

and salts. Also, the solid grey waterfront could be seen in the micrographs, which was absent in the micrographs of MYC at pH 3.0 with all 3 salts (i.e., NaCl, CaCl₂ and FePP). The lack of obvious microstructural differences in the presence of FePP and at acidic pH might be due to a low fungal protein concentration on the hyphal surface, i.e., this surface is unaffected by pH, does not ionize and so does not particularly bind Fe³⁺, although the elemental analysis (see below) suggested some surface affinity.

The elemental analysis of MYC with added 200 mM NaCl, 100 mM CaCl₂ and 1.0 mM FePP is shown in Fig. 3. Fig. 3a shows the full spectra of the relative elemental composition, with carbon and oxygen having the biggest peaks. Both peaks appear to track the positions of the hyphae. Elements from the added salts: sodium, chlorine, calcium, iron and phosphorus, shown in Fig. 3f–j, appear more evenly distributed throughout the MYC, although iron showed a slightly higher concentration coincident with the positions of the hyphae. The bright patches on the phosphorus map (Fig. 3j) appear to coincide with the brighter patches on the surface of the MYC in the cryo-SEM Fig. 3b, but this is thought to be an artefact, due to patches of iridium used in coating of the sample surface, since the phosphorus and iridium peaks overlap (Fig. 3a).

Fig. 4 shows the storage modulus (G') of MYC as a function of f (0.01, 0.1, 1 and 10 Hz) and FePP at various pH. The most striking feature is the higher values of G' at pH 3.0 at all f , irrespective of whether FePP is added or not, though the addition of FePP considerably suppresses G' at pH 3.0. Values of G' at pH 5.0 and 7.0 at the same f are mostly similar,

whilst G' versus $\log_{10} f$ between 0.01 and 10 Hz shows a similar, modest positive gradient for all systems. Because the trends with f were similar, subsequent rheological data for more the complex MYC-PoP systems (see below) are only presented for $f = 0.1$ Hz (whilst the full data set is given in Supplementary Figs. S1–S4).

Cross-linking by Ca²⁺ is thought to be responsible for maintaining the three-dimensional structure of the hyphal network and the resulting paste-like properties of MYC. The Fe³⁺ ions appear to enhance hyphal aggregation, presumably via binding to carboxylate groups of proteins and enhancing non-disulphide intermolecular interactions (Li, et al., 2009). Thus, ferric ions appear to work in synergy with acidic conditions (pH 3.0) in giving increased granular structure and syneresis of the MYC.

Reduction in G' of MYC with the addition of FePP across all measured f and pH conditions (Fig. 4) is thought to be linked to ferric-induced protein aggregation (Li, et al., 2009) on the hyphal surfaces. A low fungal protein concentration on the hyphal surface will mean that protein aggregation will disrupt the protein-mediated hyphal interactions enough to lower G' . It is thought that the protein aggregate carboxylic groups will be fully sequestered by ferric interactions and that this and the fewer available surface protein interaction sites become insufficient to maintain protein-hyphal interactions. This results in the sharp decrease in G' in the presence of FePP. The crosslinking ability of Ca²⁺ restores some of MYC's structure as measured by G' but it is insufficient to reverse the effects of ferric-induced protein aggregation as discussed further below. The more complex changes in G' of MYC with added PoP and the three salts (FePP, CaCl₂ and NaCl) at different pH are discussed

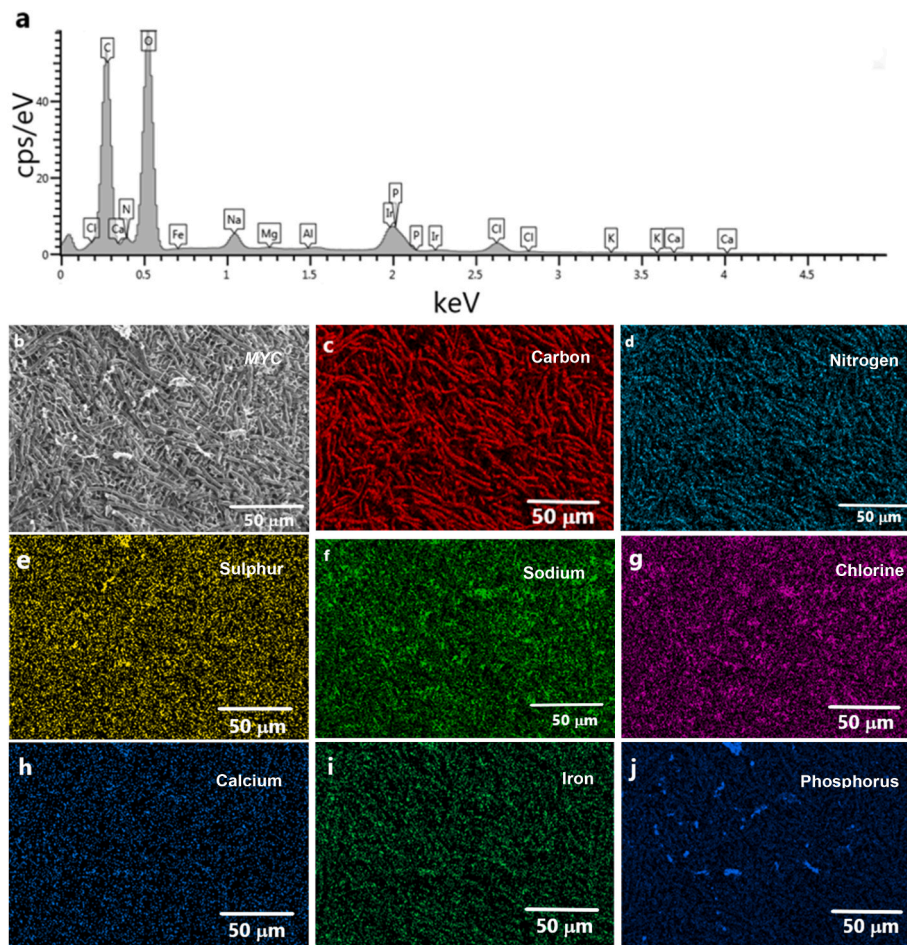


Fig. 3. Elemental map from Cryo-SEM EDX of MYC (20 wt %) with added 200 mM NaCl, 100 mM CaCl₂ and 1.0 mM Fe₄(P₂O₇)₃ at pH 5.0 showing a) relative elemental composition spectra b) fungal hyphae paste c) Carbon d) Nitrogen e) Sulphur f) Sodium g) Chlorine h) Calcium i) Iron j) Phosphorus. Scale bar represents 50 μm.

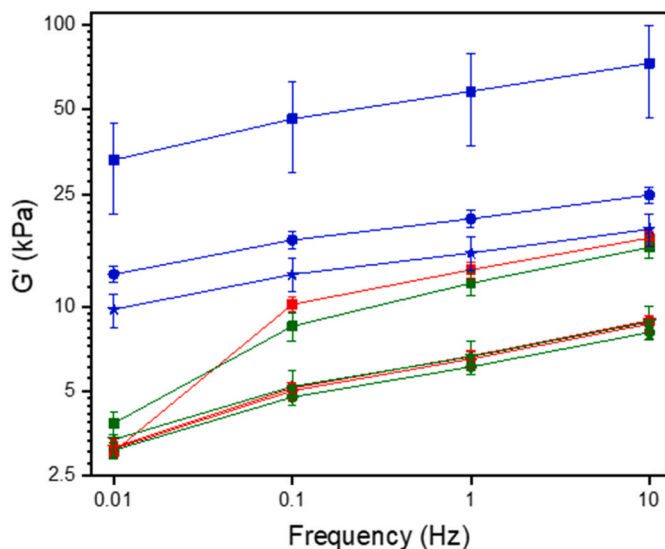


Fig. 4. Mean storage modulus (G') at 0.1% shear strain and 25 °C of MYC as a function of frequency showing G' with no added salts at pH 7.0 (■), 5.0 (■) and 3.0 (■); with 0.5 mM Fe₄(P₂O₇)₃ at pH 7.0 (●), 5.0 (●) and 3.0 (●); with 1.0 mM Fe₄(P₂O₇)₃ at pH 7.0 (★), 5.0 (★) and 3.0 (★). Error bars represent standard deviation for rheological analysis of triplicate samples (n = 3 × 3).

in depth in sections 3.3 and 3.4.

3.2. Hydrodynamic diameter (d_H) of PoP as a function of pH and Fe³⁺

Before trying to understand the effect of pH and Fe³⁺ on the more complex MYC-PoP system, the effects of Fe³⁺ on the PoP itself were investigated. Table 1 shows the hydrodynamic diameter (d_H) of PoP at pH 7.0, 5.0 and 3.0 with and without 1.0 mM FePP (hereafter referred to as PoP-Fe) filtered through a 0.22 μm filter. The measured d_H of PoP was 51.3 nm, 8.5 nm and 52.0 nm at pH 7.0, 5.0 and 3.0 respectively. The magnitude of d_H at pH 7.0 is in line with previous reports of the d_H of soluble fractions of patatin at pH 7.0 (Aery, et al., 2023). Since pH 5.0 is close to the isoelectric point of patatin, it was expected that the largest

Table 1

Mean hydrodynamic diameter (d_H) and polydispersity index of potato protein solution with and without 1.0 mM Fe₄(P₂O₇)₃. Means are shown with standard deviation for particle size measurement in triplicate of each sample (n = 3).

pH	Sample	Mean d_H (nm)	Polydispersity index (PDI)
7.0	PoP	51.3 ± 0.5 ^a	0.542 ± 0.01 ^a
5.0	PoP	8.5 ± 0.2 ^a	0.169 ± 0.01 ^a
3.0	PoP	52.0 ± 0.4 ^a	0.547 ± 0.05 ^a
7.0	PoP-Fe	42.8 ± 0.8 ^a	0.521 ± 0.03 ^a
5.0	PoP-Fe	98.4 ± 0.3 ^a	0.291 ± 0.03 ^a
3.0	PoP-Fe	510 ± 436.7 ^{*a}	0.668 ± 0.5 ^a

Means with the same letter of the alphabet in a column are not significantly different $p < 0.05$. *9 replicates for this sample.

particle size might have been observed at this pH. With a molecular weight of ~ 45 kDa, patatin's minimal radius, assuming it takes up a spherical configuration, is ~ 2.4 nm. Consequently, the d_H value of 8.5 nm measured at pH 5.0 mostly likely represents patatin dimers (Erickson, 2009), that would easily pass through the $0.22 \mu\text{m}$ filter before size measurement. This also implies that patatin aggregates much larger than this cut-off $0.22 \mu\text{m}$ size were indeed formed at this pH, so that the $d_H = 8.5$ nm value is not representative of the true patatin aggregate size at pH 5.0.

In the presence of *FePP* at pH 5.0 this apparent low d_H value increased more than 11-fold to 98.4 nm. A similar (10-fold) increase of d_H was observed at pH 3.0 with the addition of *FePP*, whereas an increase in d_H of *PoP-Fe* was not observed at pH 7.0, rather a slight (17 %) decrease. The large increases in d_H at acid pH values are obviously suggestive of significant *PoP* aggregation in the presence of Fe^{3+} and so this was likely to affect significantly the rheology of the corresponding *MYC-PoP* composite gels, as discussed below.

3.3. Microstructure of *MYC-PoP* composites as a function of pH and multivalent salts

Figs. 5 and 6 show the microstructure of the *MYC-PoP* composite across various length scales in the absence or presence of Fe^{3+} . Immunolabelled confocal micrographs of *MYC-PoP* are shown in Fig. 5. Fig. 5a and b show representative white light images of the fungal hyphae dispersed in water with Calcofluor White (which appears blue in these images) bound to chitin in the fungal cell wall. Fig. 5c provides the first evidence that *PoP*, labelled with Alexa 568 dye (which appears orange in these images) completely covers the surface of the fungal hyphae of these *MYC-PoP* meat analogues. The immunolabelling control samples shown in Supplementary Fig. S5 confirm the absence of non-specific interactions between both primary and secondary antibodies with the hyphae. Fig. 6 shows the effect of *PoP* at 3 wt % on the microstructure of *MYC* at pH 5.0 and 3.0 with and without added salts. At pH 5.0 and no added salts, the fungal hyphae appeared to have some 'webbing' on their surface. In the presence of 100 mM CaCl_2 and 200 mM NaCl , the webbing appeared to be reduced, whilst a significant increase in webbing was observed when all three salts (100 mM CaCl_2 , 200 mM NaCl and 1.0 mM *FePP*) were present together, compared to when all salts were absent. At pH 3.0, the webbing appeared to become more abundant under all conditions, with a 'granular' structure that was even more prevalent in the presence of salts. *MYC-PoP* with all three salts present is seen to produce an increase in granular structures both on and between the hyphae. This is not surprising given the aggregation of *PoP* induced by Fe^{3+} as revealed above. A more in-depth comparison of the differences in microstructure of *MYC* and *MYC-PoP* is presented in the final discussion section below.

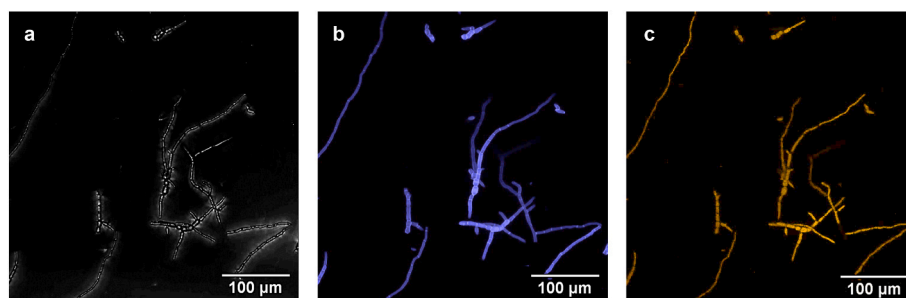


Fig. 5. Confocal micrographs of 0.1 g L^{-1} dispersion of *MYC* in 1.0 g L^{-1} dispersion of potato protein showing a) white light image of the fungal hyphae, b) chitin stained with Calcofluor White excited at 405 nm and c) potato protein labelled with anti-patatin and a corresponding secondary antibody conjugated to Alexa 568 dye excited at 578 nm. Scale bar represents $100 \mu\text{m}$.

3.4. Rheology of *MYC-PoP* as a function of pH and multivalent salts

Fig. 7 shows the comprehensive effects of *PoP*, added salts and pH on the G' of *MYC* at 0.1 Hz and 0.1% shear strain, which are comfortably within the linear viscoelastic regime. (See Supplementary Figs. S2–S4 for data at higher f , where G' increases with f but similar trends as detailed below were observed). The most obvious trends in Fig. 7 are as follows.

- In the absence of Fe^{3+} (Fig. 7a, d and g) the presence of *PoP* causes a significant reduction in G' at all added $[\text{NaCl}]$ and $[\text{CaCl}_2]$, but particularly at pH 7.0. Only at 0 mM NaCl and CaCl_2 at pH 5.0 is G' slightly higher with *PoP*, within the experimental error. There are no large or consistent changes in the effects of increasing $[\text{NaCl}]$ and $[\text{CaCl}_2]$ except that at pH 7.0 G' values tend to converge to the same value (ca. 23 kPa) without *PoP* and to a lower value (ca. 7 kPa) with *PoP*. At pH 7.0 and 5.0 without *PoP* G' is higher when $[\text{CaCl}_2]$ is higher, whereas at pH 3.0 the opposite is true and even more so when *PoP* is present. Turning to the effects of adding 0.5 or 1.0 mM *FePP*, the most noticeable effects are as follows.
- At pH 7.0 and 5.0 (Fig. 7b, c and e, f, respectively) in the absence of *PoP*, the tendency is for all G' values to be lower in the presence of Fe^{3+} ions than without Fe^{3+} and for G' values to converge and become relatively independent of $[\text{NaCl}]$. Thus Fe^{3+} somehow seems to dominate the behaviour. At the same time, increasing $[\text{CaCl}_2]$ partly mitigates against this, raising G' back up, though to values not as high as without Fe^{3+} . With Fe^{3+} in all cases, however, G' with *PoP* $>$ G' without *PoP*, pointing to some advantages (in terms of a firmer texture) of having Fe^{3+} present if *PoP* is added into the system at pH 5.0 or 7.0.
- At pH 3.0 (Fig. 7h and i) the situation is noticeably different from at pH 7.0 and 5.0. For example, with *PoP* some of the highest G' values for all the systems were recorded, notably at 0 mM NaCl and CaCl_2 . All G' values tended to decrease significantly when $[\text{NaCl}]$ and/or $[\text{CaCl}_2]$ were increased (with the exception of 0.5 mM *FePP* + 200 mM NaCl + 100 mM CaCl_2 – see Fig. 7h). In contrast, in the absence of *PoP* at both $[\text{FePP}]$, all values of G' were suppressed to similar low values and relatively unaffected by $[\text{NaCl}]$ and $[\text{CaCl}_2]$, as at pH 7.0 and 5.0.

In summary, as little as 0.5 mM *FePP* drastically weakens G' of *MYC* at pH 7.0, 5.0 or 3.0. (Further increase to 1.0 mM *FePP* produces very little further change). This highlights the extreme sensitivity of 'bare' hyphae to these low levels of Fe^{3+} ions. The opposite trend is seen with the *MYC-PoP* composite, where a strengthening of G' with addition of *FePP* occurs at all 3 pH values. At pH 7.0 and 5.0 the effects of NaCl are variable and not strong, whereas CaCl_2 tends to give a slight strengthening both types of composites, i.e., with and without *PoP*, except at pH 3.0, where a weakening effect is observed on the addition of both NaCl and CaCl_2 , especially in the presence of *FePP*.

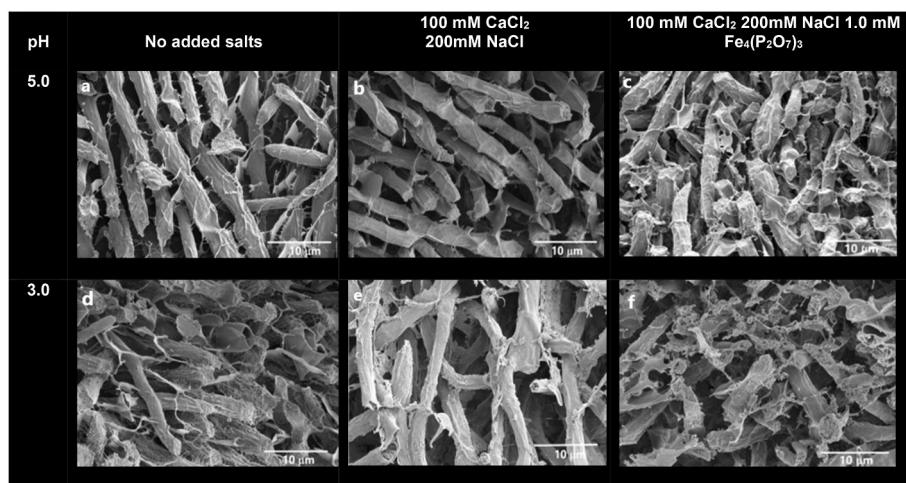


Fig. 6. Cryo-SEM image of MYC-PoP (20 wt %) at pH 5.0 with a) no added salts, b) added 200 mM NaCl and 100 mM CaCl₂, c) added 200 mM NaCl, 100 mM CaCl₂ and 1.0 mM Fe₄(P₂O₇)₃; pH 3.0 with d) no added salts, e) added 200 mM NaCl and 100 mM CaCl₂, f) added 200 mM NaCl, 100 mM CaCl₂ and 1.0 mM Fe₄(P₂O₇)₃. Scale bar represents 10 μm.

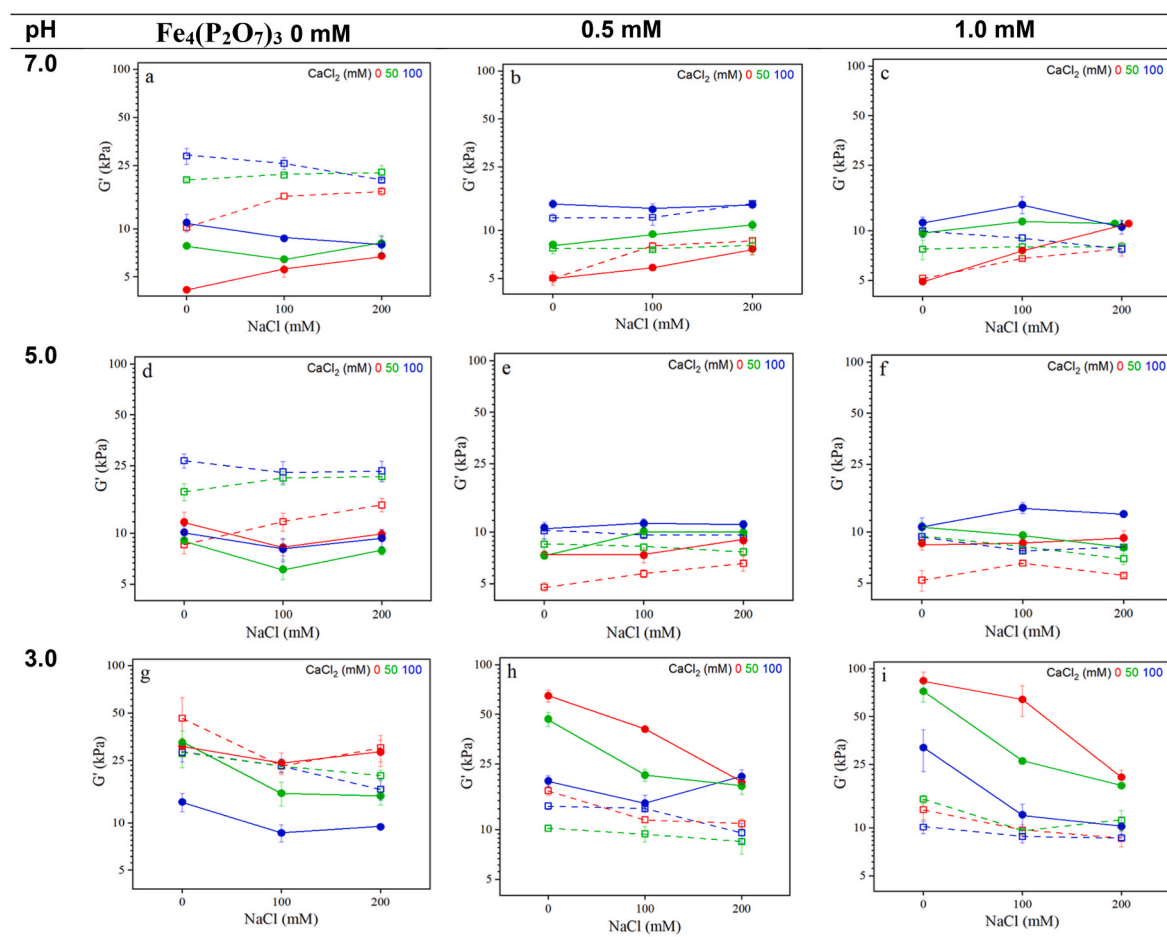


Fig. 7. Mean storage modulus (G') at 0.1% shear strain, frequency 0.1 Hz and 25 °C of MYC (□, open squares) and MYC-PoP (●, filled circles) as a function of NaCl and at 0 (red) 50 (green) and 100 mM (blue) CaCl₂. Top row (a, b and c) at pH 7.0, middle row (d, e and f) at pH 5.0, bottom row (g, h and i) at pH 3.0. First column (a, d & g) with no added Fe₄(P₂O₇)₃, middle column (b, e and h) with 0.5 mM Fe₄(P₂O₇)₃, third column (c, f and i) with 1.0 mM Fe₄(P₂O₇)₃ added. Error bars represent standard deviation for rheological analysis of triplicate samples (n = 3 × 3).

In trying to explain further the rheology of the MYC-PoP system in the context of all the other results, one should recognize that, most probably the PoP largely coats all the surfaces of the hyphae (Fig. 5). This was the conclusion of previous work (Okeudo-Cogan, et al. (2023)

using egg white protein (EWP) at the same bulk protein concentration, where the theoretical hyphal surface coverage was estimated as 33 mg m⁻² (This was assuming all the added protein was at the hyphal surface, i.e., ignoring any that remained in the bulk solution). In which case the

characteristics of *PoP* will largely determine the interactions of the hyphae covered in this protein, i.e., the *MYC-PoP* composite. The significant increase in the hyphal surface material observed with *MYC-PoP* (Fig. 6) are thought to represent aggregates of *PoP* (compare with just *MYC* in Fig. 2). A key result is that addition of *PoP* greatly reduced the G' for all samples in the absence of *FePP*. This should be compared with only a slight weakening of G' when *EWP* was added to *MYC* instead. This indicates significant differences in the interactions between the hyphae when *PoP* is present on the hyphal surface as binder, as opposed to *EWP* (Okeudo-Cogan, et al., 2023).

CaCl_2 generally fosters cross-linking and structuring of proteins and the increase in G' and surface material decorating the hyphal surfaces and inter-hyphal spaces when CaCl_2 was added is evidence of this here. The inter-hyphal particulate material seen in the cryo-SEM images (Fig. 6c, f) is probably mostly *PoP* aggregates when Fe^{3+} was added. At pH 5.0 a more than 11-fold apparent increase in d_H of *PoP* was observed when *FePP* was added to *PoP* alone (Table 1). This aggregation may be due to a combination of specific ferric-induced protein-protein interactions and the minimal net charge of patatin when close to its isoelectric point (pH 4.5 to 5.1) (Andlinger, et al., 2021; Li et al., 2009). At pH 3.0 d_H was even higher, again probably due to Fe^{3+} crosslinking, but possibly also due to *PoP* denaturation as well (Schmidt, et al., 2019). The material observed between the hyphae also appeared to aggregate further at pH 3.0: presumably this is also *PoP*.

The obvious dependency of G' of both *MYC* and *MYC-PoP* on the ionic make-up of the solutions at all 3 pH values indicates electrostatic interactions as the main type of force operating within the *MYC-PoP* composites, as it was for *MYC-EWP* composites (Okeudo-Cogan, et al., 2023). However, in addition to the general charge screening effects by these ions and possible Ca^{2+} -mediated specific cross-linking, ferric ions enhance aggregation of *PoP* and/or native fungal proteins, both on the surface of the hyphae but also in the inter-hyphal spaces (see Fig. 6f) where most protein aggregates appear. Overall, this results in a decrease in G' for *MYC* with and without added *PoP* in the absence of added Na^+ and Ca^{2+} at pH 5.0 and 7.0 whilst the opposite trend is observed at pH 3.0 where protein aggregation is thought to dominate attractive interactions between the hyphae. Thus, unlike Fe^{3+} alone, Ca^{2+} and Fe^{3+} when present together improved (i.e. raised) the stiffness of *MYC-PoP* more than *MYC*. Despite the initial decrease in G' of *MYC* with the addition of *PoP*, interactions of *PoP* with Fe^{3+} plus Ca^{2+} further increased G' of the composite. Thus Ca^{2+} and Fe^{3+} acted synergistically on *MYC-PoP* in enhancing the stiffness of the matrix of hyphae coated in *PoP*, moving this composite a little closer to the properties *MYC-EWP*. For example, at pH 7.0 and 100 mM CaCl_2 , G' of *MYC-PoP* + 0.5 mM *FePP* was 14.6 kPa, compared to 22.7 kPa of *MYC-EWP* without *FePP* (Okeudo-Cogan, et al., 2023).

4. Conclusions

Potato protein (*PoP*) has been used as a replacement of egg white protein (*EWP*) as binder in a model fungal-based meat alternative. *PoP*, like *EWP*, was shown to coat the fungal hyphae surface but cf. *EWP* conferred a significant reduction in stiffness (as measured by the storage modulus G'). Fe^{3+} added as ferric pyrophosphate (*FePP*) was seen to give a more reddish-brown colour, reduce G' and enhance aggregation of fungal hyphae paste, particularly at low pH, via protein-protein aggregation. Overall the structuring role of Ca^{2+} seems to dominate its influence, whilst the main effect of Fe^{3+} is protein aggregation, which in systems with lower bulk protein content results in loss of inter-hyphal interaction and composite strength. The co-addition of ferric and calcium salts to mycoprotein + potato protein composite (*MYC-PoP*) on the other hand, produced superior rheological and structural properties, such as reduction in protein aggregation and increase in G' relative to the *MYC* alone. This study thus offers new insights into the effects of fortification of vegan meat alternatives where synergistic interactions of various micronutrients, specifically divalent and trivalent cations, may

compensate for any textural weakening caused by addition of plant proteins. Further work is needed to understand how these changes are impacted by processing such as heating, freezing and cold storage of the fungal-plant protein based meat analogue, since these changes to G' of *MYC* in the presence of *PoP* might become more profound following such processing. In addition, further work will be required to compare the effects on these model systems with their effects on real commercial MAs with a view to mimicking real meat products.

Author contributions

Mary C. Okeudo: Conceptualization, Methodology, Investigation, Formal analysis, Writing – original draft; Anwasha Sarkar: Conceptualization, Writing – review & editing, Supervision; Brent S. Murray: Conceptualization, Writing – review & editing, Supervision; Rammile Ettelaie: Conceptualization, Writing – review & editing, Supervision; Richa Yeshvekar: Methodology, Investigation; Shuyue Yang: Investigation; Simon D. Connell: Conceptualization, Writing – review & editing, Supervision; Stewart Radford: Conceptualization, Supervision; Stuart Micklethwaite: Methodology, Investigation; Yoselin Benitez Alfonso: Methodology, Investigation.

Declaration of competing interest

We confirm that there would be no conflicting interests regarding publication of, “Multivalent cations modulating microstructure and interactions of potato protein and fungal hyphae in a functional meat analogue”.

Data availability

Data will be made available on request.

Acknowledgements

Authors gratefully acknowledge the Engineering and Physical Sciences Research Council (EPSRC) funded Centre for Doctoral Training in Molecules to Product, Grant Ref. No. EP/S022473/1 as well as Quorn, UK for financial support. Prof. Yoselin Benitez-Alfonso and Dr. Richa Yeshvekar acknowledge UK Research and Innovation council (MR/T04263X/1) for their support. We would also like to thank Dr. Ruth Hughes at the Bioimaging Facility, University of Leeds, for access and assistance with confocal microscopy.

Appendix A. Supplementary data

Supplementary data to this article can be found online at <https://doi.org/10.1016/j.foodhyd.2023.109569>.

References

- Aery, S., Parry, A., Araiza-Calahorra, A., Evans, S. D., Gleeson, H. F., Dan, A., et al. (2023). Ultra-stable liquid crystal droplets coated by sustainable plant-based materials for optical sensing of chemical and biological analytes. *Journal of Materials Chemistry C*, 11(17), 5831–5845.
- Andlinger, D. J., Röscheisen, P., Hengst, C., & Kulozik, U. (2021). Influence of pH, temperature and protease inhibitors on kinetics and mechanism of thermally induced aggregation of potato proteins. *Foods*, 10(4), 796.
- Baltic, M. Z., & Boskovic, M. (2015). When man met meat: Meat in human nutrition from ancient times till today. *Procedia Food Science*, 5, 6–9.
- Bevan, M., Barker, R., Goldsbrough, A., Jarvis, M., Kavanagh, T., & Iturriaga, G. (1986). The structure and transcription start site of major potato tuber protine gene. *Nucleic Acids Research*, 14(11), 4625–4638.
- Cabrera, M. C., Ramos, A., Saadoun, A., & Brito, G. (2010). Selenium, copper, zinc, iron and manganese content of seven meat cuts from Hereford and Braford steers fed pasture in Uruguay. *Meat Science*, 84(3), 518–528.
- Cercamondi, C. I., Duchateau, G. S. M. J. E., Harika, R. K., van den Berg, R., Murray, P., Koppenol, W. P., et al. (2016). Sodium pyrophosphate enhances iron bioavailability from bouillon cubes fortified with ferric pyrophosphate. *British Journal of Nutrition*, 116(3), 496–503.

- Chen, Y., Wang, C., Chang, T., Shi, L., Yang, H., & Cui, M. (2014). Effect of salts on textural, color, and rheological properties of potato starch gels. *Starch*, 66(1–2), 149–156.
- Creusot, N., Wierenga, P. A., Laus, M. C., Giuseppin, M. L., & Gruppen, H. (2011). Rheological properties of patatin gels compared with β -lactoglobulin, ovalbumin, and glycinin. *Journal of the Science of Food and Agriculture*, 91(2), 253–261.
- Czerwonka, M., & Tokarz, A. (2017). Iron in red meat—friend or foe. *Meat Science*, 123, 157–165.
- Desimone, T. L., Acheson, R. A., Woerner, D. R., Engle, T. E., Douglass, L. W., & Belk, K. E. (2013). Nutrient analysis of the beef alternative merchandising cuts. *Meat Science*, 93(3), 733–745.
- Erickson, H. P. (2009). Size and shape of protein molecules at the nanometer level determined by sedimentation, gel filtration, and electron microscopy. *Biological Procedures Online*, 15(11), 32–51.
- Finnigan, T. J. A. (2011). Mycoprotein: Origins, production and properties. In G. O. Phillips, & P. A. Williams (Eds.), *Handbook of food proteins* (pp. 335–352). Cambridge: Woodhead Publishing.
- Finnigan, T., Needham, L., & Abbott, C. (2017). Mycoprotein: A healthy new protein with a low environmental impact. In S. R. Nadathur, J. P. D. Wanasundara, & L. Scanlin (Eds.), *Sustainable protein sources* (pp. 305–325). San Diego: Academic Press.
- Finnigan, T. J. A., Wall, B. T., Wilde, P. J., Stephens, F. B., Taylor, S. L., & Freedman, M. R. (2019). Mycoprotein: The future of nutritious nonmeat protein, a symposium review. *Current Developments in Nutrition*, 3(6), nzz021.
- Grubben, N. L. M., van Heeringen, L., & Keesman, K. J. (2019). Modelling potato protein content for large-scale bulk storage facilities. *Potato Research*, 62(3), 333–344.
- Guha, S., Majumder, K., & Mine, Y. (2019). Egg proteins. In L. Melton, F. Shahidi, & P. Varela (Eds.), *Encyclopedia of food chemistry* (pp. 74–84). Oxford: Academic Press.
- Hou, Y., Xu, X., Hu, W., Pei, H., Chen, H., Tong, P., et al. (2021). Effect of L-calcium lactate, zinc lactate, and ferric sodium EDTA on the physicochemical and functional properties of liquid whole egg. *Journal of Food Science*, 86(9), 3839–3854.
- Hussain, M., Qayum, A., Xiuxiu, Z., Liu, L., Hussain, K., Yue, P., et al. (2021). Potato protein: An emerging source of high quality and allergy free protein, and its possible future based products. *Food Research International*, 148, Article 110583.
- Institute of Medicine Committee. (1993). In *Iron Deficiency Anemia: Recommended Guidelines for the Prevention, Detection, and Management Among U.S. Children and Women of Childbearing Age*. Washington (DC: National Academies Press (US).
- Kew, B., Holmes, M., Stieger, M., & Sarkar, A. (2021). Oral tribology, adsorption and rheology of alternative food proteins. *Food Hydrocolloids*, 116, Article 106636.
- Li, C., Fu, X., Qi, X., Hu, X., Chasteen, N. D., & Zhao, G. (2009). Protein association and dissociation regulated by ferric ion: A novel pathway for oxidative deposition of iron in pea seed ferritin. *Journal of Biological Chemistry*, 284(25), 16743–16751.
- Melville, H., Shahid, M., Gaines, A., McKenzie, B. L., Alessandrini, R., Trieu, K., et al. (2023). The nutritional profile of plant-based meat analogues available for sale in Australia. *Nutrition and Dietetics*, 80(2), 211–222.
- Micheletto, M., Gaio, E., Tedesco, E., Di Maira, G., Mantovan, E., Zanella, M., et al. (2022). Intestinal absorption study of a granular form of ferric pyrophosphate. PMC9145852 *Metabolites*, 12(5), 463.
- Moretti, D., Zimmermann, M. B., Wegmüller, R., Walczyk, T., Zeder, C., & Hurrell, R. F. (2006). Iron status and food matrix strongly affect the relative bioavailability of ferric pyrophosphate in humans. *The American Journal of Clinical Nutrition*, 83(3), 632–638.
- Okeudo-Cogan, M. C., Murray, B. S., Ettelaie, R., Connell, S. D., Radford, S. J., Micklethwaite, S., et al. (2023). Understanding the microstructure of a functional meat analogue: Demystifying interactions between fungal hyphae and egg white protein. *Food Hydrocolloids*, 140, Article 108606.
- Schmidt, J. M., Damgaard, H., Greve-Poulsen, M., Sunds, A. V., Larsen, L. B., & Hammershøj, M. (2019). Gel properties of potato protein and the isolated fractions of patatins and protease inhibitors – impact of drying method, protein concentration, pH and ionic strength. *Food Hydrocolloids*, 96, 246–258.
- Sharratt, W. N., Lopez, C. G., Sarkis, M., Tyagi, G., O'Connell, R., Rogers, S. E., et al. (2021). Ionotropic gelation fronts in sodium carboxymethyl cellulose for hydrogel particle formation. *Gels*, 7(2), 44.
- Tian, T., Blanco, E., Smoukov, S. K., Velev, O. D., & Velikov, K. P. (2016). Dissolution behaviour of ferric pyrophosphate and its mixtures with soluble pyrophosphates: Potential strategy for increasing iron bioavailability. *Food Chemistry*, 208, 97–102.
- Wiebe, M. G. (2004). Quorn™ Myco-protein - overview of a successful fungal product. *Mycologist*, 18(1), 17–20.